Understanding Recent Eastern Horn of Africa Rainfall Variability and Change

BRANT LIEBMANN,* MARTIN P. HOERLING,+ CHRIS FUNK,# ILEANA BLADÉ,@ RANDALL M. DOLE,+ DAVE ALLURED,* XIAOWEI QUAN,* PHILIP PEGION,* AND JON K. EISCHEID*

* *NOAA/Earth System Research Laboratory, and Cooperative Institute for Research in Environmental Sciences, University of Colorado, Boulder, Colorado*
+ *NOAA/Earth System Research Laboratory, Physical Sciences Division, Boulder, Colorado*
# *U.S. Geological Survey, Earth Resources Observation and Science Center, Sioux Falls, South Dakota, and the Climate Hazards Group, University of California, Santa Barbara, Santa Barbara, California*
@ *Departament d'Astronomia i Meteorologia, Facultat de Física, Universitat de Barcelona, and Institut Català de Ciències del Clima, IC3, Barcelona, Spain*

(Manuscript received 22 November 2013, in final form 21 April 2014)

ABSTRACT

Observations and sea surface temperature (SST)-forced ECHAM5 simulations are examined to study the seasonal cycle of eastern Africa rainfall and its SST sensitivity during 1979–2012, focusing on interannual variability and trends. The eastern Horn is drier than the rest of equatorial Africa, with two distinct wet seasons, and whereas the October–December wet season has become wetter, the March–May season has become drier.

The climatological rainfall in simulations driven by observed SSTs captures this bimodal regime. The simulated trends also qualitatively reproduce the opposite-sign changes in the two rainy seasons, suggesting that SST forcing has played an important role in the observed changes. The consistency between the sign of 1979–2012 trends and interannual SST–precipitation correlations is exploited to identify the most likely locations of SST forcing of precipitation trends in the model, and conceivably also in nature. Results indicate that the observed March–May drying since 1979 is due to sensitivity to an increased zonal gradient in SST between Indonesia and the central Pacific. In contrast, the October–December precipitation increase is mostly due to western Indian Ocean warming.

The recent upward trend in the October–December wet season is rather weak, however, and its statistical significance is compromised by strong year-to-year fluctuations. October–December eastern Horn rain variability is strongly associated with El Niño–Southern Oscillation and Indian Ocean dipole phenomena on interannual scales, in both model and observations. The interannual October–December correlation between the ensemble-average and observed Horn rainfall 0.87. By comparison, interannual March–May Horn precipitation is only weakly constrained by SST anomalies.

1. Introduction

The eastern Horn of Africa (hereinafter ''Horn'') is isolated from the rest of the continent by a chain of mountains that includes the highest elevations of Africa and is interrupted only by the relatively low Turkana basin of Kenya, which extends northwestward into Sudan (Fig. 1). The climate of the eastern Horn is also unusual, with total annual precipitation being substantially lower than in the rest of equatorial Africa (e.g., Hoerling et al. 2006) and with an annual cycle characterized by two distinct wet seasons, with little to no precipitation in between (e.g., Liebmann et al. 2012). The primary agricultural season, which is in the northern hemisphere spring, is usually considered the ''long'' rainy season and is also more reliable than the northern hemisphere fall ''short'' rainy season. Indeed, crop failure in the fall season occurs as often as once every 3 yr (e.g., Hutchinson 1992).

Local rains in the eastern Horn are the primary water source for agriculture, there being limited groundwater, streamflow from remote regions, and reservoir storage. It is thus of great concern and consequence that rains during the long rainy season have declined since 1979. This situation has also highlighted the need to improve predictions of the short and long rains, including

Corresponding author address: Brant Liebmann, CIRES, University of Colorado, Campus Box 216, Boulder, CO 80309.
E-mail: brant.liebmann@noaa.gov

DOI: 10.1175/JCLI-D-13-00714.1

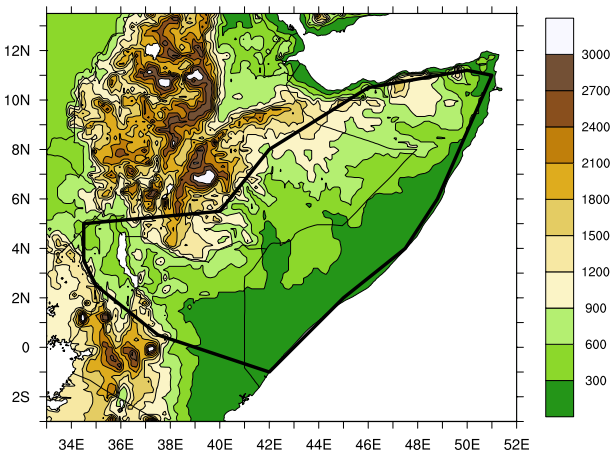

FIG. 1. Elevation in meters. Polygon represents the Horn region analyzed in study.

a dynamical explanation for the drying, which would increase the ability of early warning systems to identify potential future droughts. This capacity would then allow them to preposition humanitarian assistance and develop more effective contingency plans. This paper represents an effort toward both of those goals.

It is has been previously established that, on interannual time scales, the short rain season exhibits a relationship with El Niño–Southern Oscillation (ENSO), with El Niño conditions being associated with above-average rainfall (Ogallo et al. 1988; Kiladis and Diaz 1989; Hutchinson 1992; Hastenrath 2000; Indeje et al. 2000; Mason and Goddard 2001). The Indian Ocean also plays a role in short rain variability, arguably more important than that of ENSO (Behera et al. 2005). Anomalously warm sea surface temperatures (SSTs) in the western equatorial Indian Ocean, together with cold SSTs in the east, centered at about 5°S—a pattern known as the Indian Ocean dipole (IOD)—force anomalous southeasterly trade winds that increase moisture supply into the coastal plain, enhancing rainfall there (Saji et al. 1999), with the western pole being of primary importance (Ummenhofer et al. 2009). This association was not evident before the 1960s and has been strongest since the late 1990s (Manatsa and Behera 2013). Black et al. (2003) showed the relationship to be nonlinear, since extreme rainfall events occur only when the gradient in absolute SST (usually from west to east) is reversed. There is also uncertainty as to whether ENSO and the IOD are independent phenomena (e.g., Goddard and Graham 1999; Saji et al. 1999; Webster et al. 1999; Black et al. 2003; Shinoda et al. 2004; Behera et al. 2005).

While substantial variability of East African short season rainfall can be explained by the IOD and ENSO, the sources of variability in long rains are proving difficult to pin down (Ogallo et al. 1988; Indeje et al. 2000; Camberlin and Philippon 2002; Camberlin and Okoola 2003). Several studies have documented a recent decline in spring (long wet season) precipitation (Funk et al. 2005, 2008; Williams and Funk 2011; Lyon and DeWitt 2012; Funk et al. 2013), which has been attributed to concurrent increases in the SST of the tropical western Pacific (Williams and Funk 2011; Lyon and DeWitt 2012; Lott et al. 2013). In this paper we will show that the drying has affected all areas of the Horn and we will assess the role of oceanic warming in greater detail. In contrast, fall wet season precipitation will be shown to have increased, in agreement with Funk and Verdin (2010).

This paper will analyze trends and interannual variability over the eastern Horn of Africa during both the short and long rainy seasons for the period 1979–2012. It will then examine the ability of a 40-member ensemble simulation with an atmospheric general circulation model (AGCM), run with specified observed SSTs, to reproduce the observational findings. To identify the oceanic regions most likely to have contributed to the changes in SST, we will examine the consistency between the precipitation and SST trends and the covariability on interannual time scales.

2. Observed and model data

Two monthly observational precipitation datasets are used in this study. The Global Precipitation Climatology Centre (GPCC) provides gridded land precipitation estimates based solely on station data. The 1° version is used in the present study (Schneider et al. 2011, 2014). It consists of the version 6 (V6) product through 2010 and the monitoring product (fewer but more up-to-date stations) through 2012. The gauge data are weighted based on the inverse distance from the grid point (Shepard 1968; Willmott et al. 1985). The second dataset is the Global Precipitation Climatology Project (GPCP). It is a combination of data from several different satellites and Global Historical Climate Network (GHCN) and Climate Anomaly Monitoring System (CAMS) data before 1986, and GPCC data thereafter (Huffman et al. 1997; Adler et al. 2003; Huffman et al. 2009). No microwave-based estimates were used prior to 1987 (Adler et al. 2003). The monthly GPCP data are available at 2.5° resolution.

The quality of precipitation analysis depends critically on the availability of station data. Even during the best-sampled period (1980–90), ground-based observations are sparse (fewer than 40 a month) in the eastern Africa region (Fig. 2), leading to substantial spatial sampling inhomogeneity. Even when more than 30 stations report per month, from about 1955 to 1990, they are concentrated

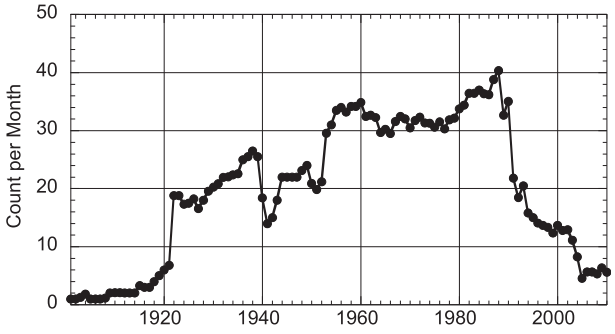

FIG. 2. Annual average monthly number of station reports used by GPCC for each year (through 2010) within the Horn region (shown in Fig. 1).

in the south and southwestern parts of the domain. Lately there have been fewer than 10 observations per month. The fact that there is an excellent correspondence between GPCC and satellite-augmented GPCP data gives some measure of confidence in the observations—although it should be kept in mind that the two datasets are far from independent. Additionally, recent studies based on denser networks of national-level station data provide separate confirmation of the long wet season precipitation declines reported in this study (Funk et al. 2012; Viste et al. 2013).

The model utilized in this study is the ECHAM5 atmospheric model (Roeckner et al. 2006), run at spectral T159 resolution (~1° in latitude and longitude). This high spatial resolution is critical for properly representing the terrain effects on rainfall over East Africa (Fig. 1). The only constraining information representing observed conditions in the ECHAM5 simulations is the SST and sea ice distribution and the external radiative forcing associated with greenhouse gases (CO_2, CH_4, O_3, and NO_2) and chlorofluorocarbons. These are specified as time-evolving monthly boundary conditions or forcing agents from January 1979 to December 2012. Climate simulations of this type are referred to as Atmospheric Model Intercomparizon Project (AMIP)-style experiments and are designed to isolate the component of atmospheric variability driven by oceanic boundary forcing. In spite of the limitations (i.e., the implied infinite oceanic heat capacity) of AMIP-style experiments (Wang et al. 2005; Hurrell et al. 2008), they remain the best option for studying SST forcing of low-frequency atmospheric variability because simulated SSTs in coupled models that include a dynamic ocean do not track those observed on an interannual basis.

Key to this modeling technique for assessing the impact of boundary conditions is an ensemble approach, whereby the simulation is repeated several times, starting each run from slightly different initial conditions but identical boundary conditions. Four sets of 10-member ensembles were performed. One employs the full forcing variability described above, the second set is identical except sea ice is kept fixed to a climatological seasonal cycle, the third has full forcing except ozone is fixed to a climatological seasonal cycle, and the fourth has full forcing except all greenhouse gases are fixed to a climatological seasonal cycle. For the present purposes, these four sets of experiments have been verified to be indistinguishable and are considered to be a single 40-member ensemble. All references to model results then refer to the ensemble mean unless otherwise specified.

The prescribed SSTs are derived from an observational dataset developed for boundary forcing experiments with uncoupled models (Hurrell et al. 2008). It is a merger of monthly mean values of SST and sea ice coverage from the Hadley Centre Sea Ice and SST (HadISST) dataset version 1.1 through 1981 (Rayner et al. 1996) with version 2 of the National Oceanic and Atmospheric Administration (NOAA) weekly optimum interpolation SST analysis (Reynolds et al. 2002). Winds are from the National Centers for Environmental Prediction (NCEP)–U.S. Department of Energy (DOE) reanalysis (NCEP-2; Kanamitsu et al. 2002).

3. Results

a. *Climatology and seasonal cycle*

Total annual climatological precipitation estimates for GPCP, ECHAM5, and GPCC for 1979–2012 (the common period between model and observations) are shown in Fig. 3. Large amounts fall over the mountains but values on the plain generally do not exceed 500 mm, while the northeast Horn is semiarid. The ECHAM5 model (Fig. 3b) reproduces the annual climatology reasonably well, both spatially and quantitatively. Key features captured by the model are the maxima over the mountains and the steep gradient toward prevailing dryness on the plain, with the northeastern Horn being drier than the southeastern Horn.

Monthly climatologies averaged over the four regions outlined in Fig. 3 are shown in Fig. 4. The Ethiopian highlands (Fig. 4a) exhibit a single summertime peak, synchronous with the timing of the wet season throughout Sudano–Sahelian Africa (Liebmann et al. 2012), with excellent agreement between the model and both observational datasets. In contrast, the second harmonic of the annual cycle becomes large relative to the first throughout the region east of the mountains as well as in the Turkana basin (Figs. 4b–d). In particular, these regions exhibit distinct double wet seasons, with comparable peaks in spring and fall. There is good general

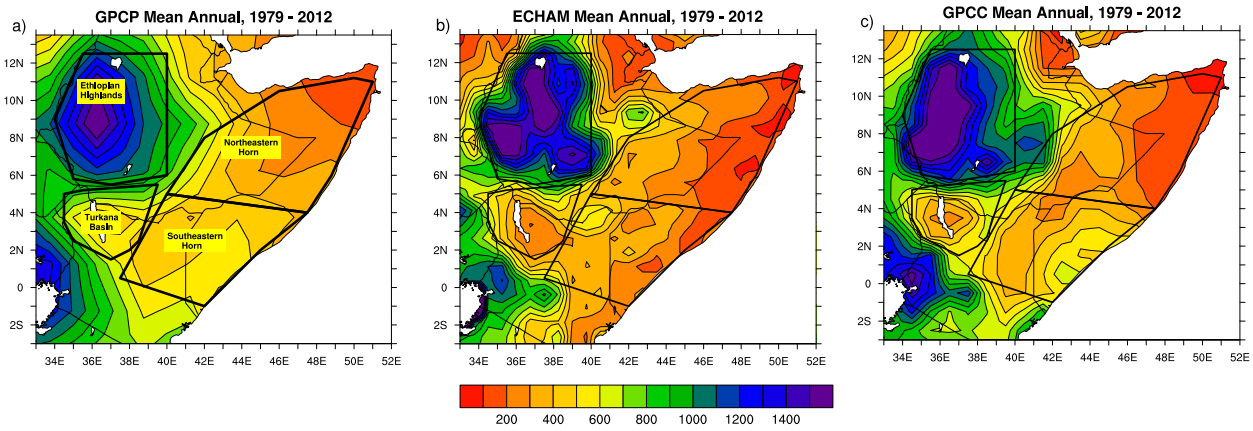

FIG. 3. Average total annual precipitation (mm) for 1979–2012 for (a) GPCP, (b) ECHAM, and (c) GPCC. Polygons indicate areas over which precipitation data are averaged.

correspondence between the seasonal cycles in observations and in the model, including the larger rainfall totals in spring relative to fall—although model rainfall is typically lower than observed, especially in fall, by about 30%.

b. *Recent change in Horn precipitation*

Figure 5 shows the percent change (relative to mean seasonal climatology) in March–May and October–December total rainfall during 1979–2012 over eastern Africa for each of the datasets, where change is defined as the least squares fit linear trend multiplied by the length of the series, in this case 34 yr. All three datasets indicate that precipitation has decreased over the Horn region during the long March–May rainy season (Figs. 5a–c), although the model change is more modest and spatially uniform than the observed estimate. Estimates of statistical significance are obtained by ranking the absolute value of the change to that of 1000 randomizations of the time series at each grid point. The 90% contour is shown in Fig. 5. The significance tends to exceed that level when the percent change is large, which is mainly over the central and southern Horn in observations, and most of the region in the model.

For the October–December short rain season (Figs. 5d–f), both observational datasets concur that precipitation has increased throughout the Horn region. The model change is also upward, but with a smaller percent increase and more uniform pattern than observations. The 90% level of significance is exceeded in a few areas near the coast in observations and almost nowhere in the model.

Time series of seasonal totals for each of the double-wet-season regions are shown in Fig. 6. A distinct drying trend is evident during March–May in each of the regions and for both observations and model (Figs. 6a–c). In the observations, spring 1981 (near the beginning of the studied period) was particularly wet over all regions; nevertheless, progressive drying is evident even disregarding this extreme season. An equally pronounced wet trend occurs during October–December in the observations (Figs. 6d,f). Note the extremely wet conditions observed during 1997 when both the strongest El Niño (in terms of Niño-3.4) and the largest IOD event (largest east-to-west temperature gradient) of the record occurred. The model precipitation for this year is also the wettest among all 34 yr of the simulation, although substantially weaker in magnitude than observations.

All three regions with a dual wet season regime have a similar annual cycle (Fig. 4); moreover, for each wet season, they display a change of the same sign over the study period (Figs. 5 and 6) and their precipitation time series bear a qualitative resemblance to each other (Fig. 6). Therefore, a larger polygon that includes these three regions is defined and the precipitation average over that polygon (shown in Fig. 1) will henceforth be called the Horn index. Furthermore, since the correlation between GPCC and GPCP Horn indices is 0.96 for March–May and 0.99 for October–December, hereafter GPCC will be referred to as ''observations.'' On average the GPCC seasonal total is lower than GPCP by 21 and 14 mm, respectively.

For reference, this Horn index is shown in Figs. 7a and 7b. Note how the model's weaker-than-observed March–May trend arises from its failure to reproduce the extraordinarily wet 1981 anomaly, but the magnitudes of the ensemble-mean precipitation totals are otherwise within the observed range. Using the same Monte Carlo randomization technique as described above, trends for all series are found to be larger than 97% of the randomized trends (see also the Fig. 7 caption). For the October–December season, instead, the model systematically

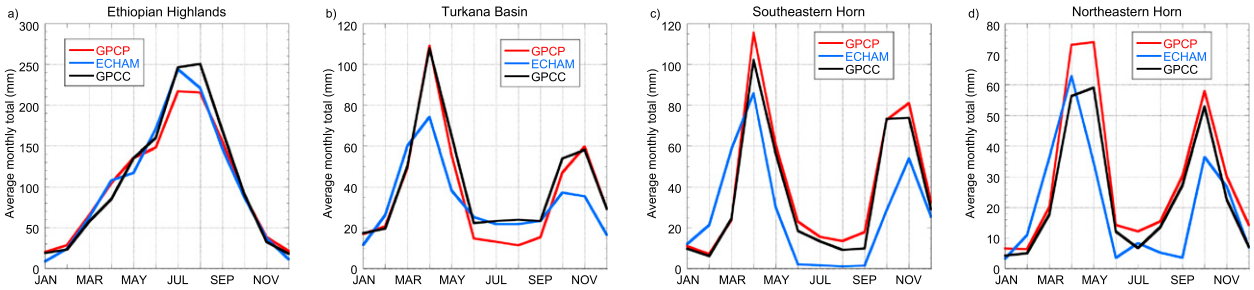

FIG. 4. Average monthly precipitation (mm) from 1979 to 2012 over regions outlined in Fig. 3.

underestimates the observed totals, although the precipitation change expressed in percent relative to the seasonal mean (Fig. 5e) is closer to the observed (not shown). All October–December changes are less significant than the March–May changes as they exceed only 75% of the randomized changes. On the other hand, the (undetrended) correlation between the ECHAM ensemble average and GPCC is 0.87 for October–December but only 0.28 for March–May.

c. *Oceanic forcing of Horn precipitation variability and recent trends*

Observed 1979–2012 SST changes for the March–May and October–December seasons are shown in Fig. 8. The patterns of change in these two seasons are qualitatively similar: the Indian and western Pacific Oceans have warmed while the eastern Pacific has cooled, more so in October–December than in March–May. The unequal changes across the Pacific in both seasons, implying an increase in the east-to-west SST gradient, are consistent with the strengthening of the Pacific Walker circulation (increased convection and rising motion in the western Pacific and subsidence in the east) that is inferred to have occurred on recent 30–40-yr time scales on the basis of observed changes in sea level pressure (L'Heureux et al. 2013). Despite the similar patterns of SST change, the precipitation trends in the Horn area have opposite signs. For this reason, we analyze the changes in the two seasons separately.

1) LONG SEASON (MARCH–MAY)

March–May average zonal winds (averaged from the equator to 15°N) from Africa to South America exhibit a good agreement between ECHAM5 (Fig. 9a) and NCEP (Fig. 9b). Over the Pacific, upper-level westerlies and lower-level easterlies are evident, consistent with a longitudinal, or Walker circulation forced by diabatic heating over the warm SSTs of the western Pacific. Over the eastern Indian Ocean, instead, there are upper-level easterlies, stronger in NCEP than ECHAM, while low-level winds are weak, also consistent with a zonal Walker cell. The 1979–2012 changes (Figs. 9c,d) reveal enhanced upper-level westerlies over the Pacific and an enhanced easterly component over Indonesia and the Indian Ocean in both ECHAM and NCEP, although in ECHAM the latter are stronger and more coherent than in NCEP. Both changes, and in particular a maximum intensification of the westerlies coincident with the presumed increase in convection (about 120°E), are consistent with the nonlinear response to localized diabatic heating (e.g., Hendon 1986).

While an empirical analysis of observations alone cannot be used to conclude that SST changes caused the changes in Horn precipitation, the fact that the ECHAM model reproduces the observed decrease in rainfall when forced with observed SSTs supports such a conclusion. Moreover, the multimodeling AMIP-type study of Lyon and DeWitt (2012), in which Horn precipitation averaged over 1999–2009 was found to be lower than in the period 1979–99, provides additional evidence for such a causal connection during the long rainy season.

Yet, the drying over the Horn is not a deterministic response to the SST forcing as there are substantial variations among ensemble members. Figure 10a is a histogram showing the March–May Horn precipitation change for each of the 40 simulations, as well as the observed change. The observed changes lie well within the range of the model spread, with some runs yielding even stronger drying than observed. The number of simulations that agree in sign with the observations (37 of 40) lends stronger evidence that the SST changes are responsible for the observed decrease in precipitation. However, a few runs (3) yielded increasing rainfall during 1979–2012. The implication is that, whereas the most probable outcome was for a drying, owing to a strong constraining effect by the SST anomalies, atmospheric noise could have led to a significantly different outcome in the single realization of nature: more or less severe drying or even no drying.

Our conclusion that the 1979–2012 SST changes have played a role in driving the observed Horn precipitation

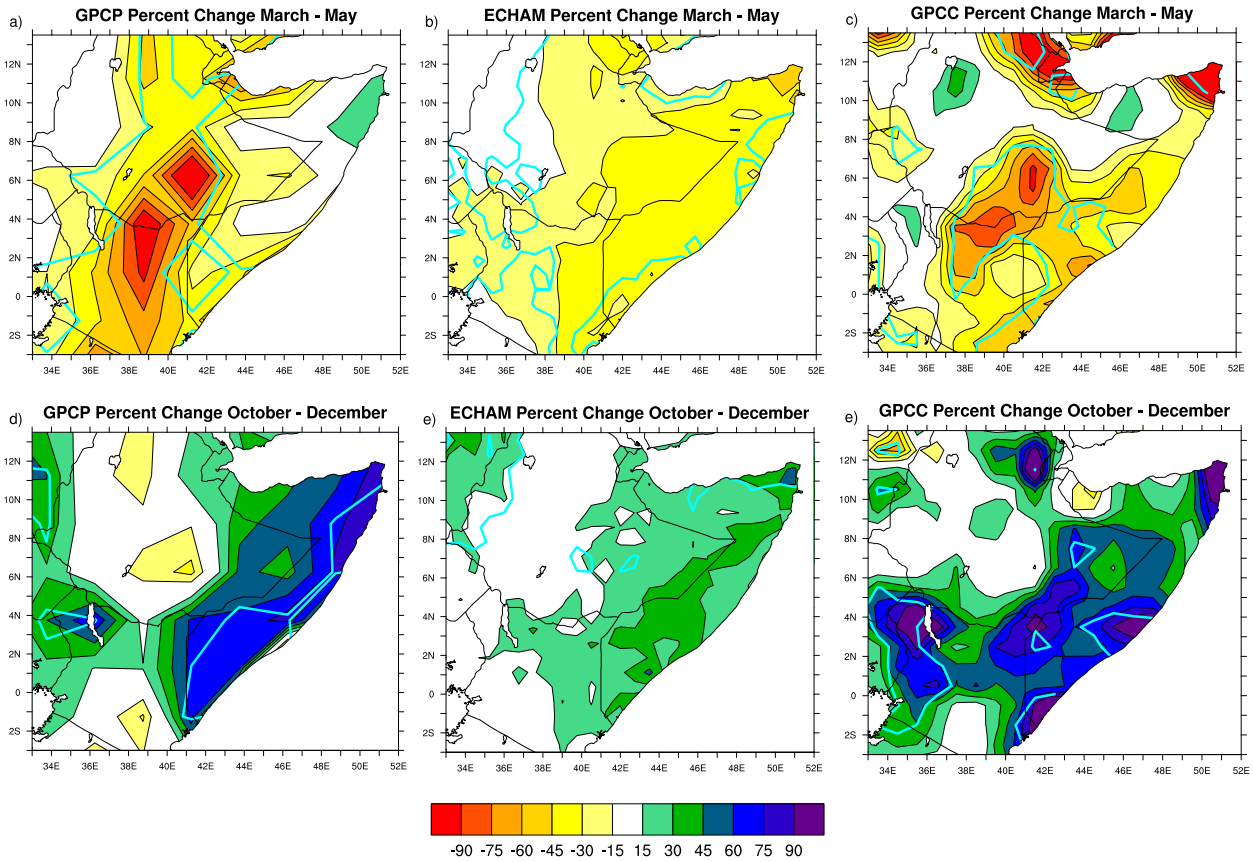

FIG. 5. Percent precipitation change (trend × 34 yr) relative to 1979–2012 average for (top) March–May and (bottom) October–December: (a) GPCP, (b) ECHAM, and (c) GPCC. Cyan curves represent the 90% statistical significance level, as determined from a 1000-randomization Monte Carlo test.

changes should be in agreement with relationships between rainfall and SST on interannual time scales, provided that the same physical mechanisms operate on both scales. If an SST trend in a region influences rainfall in another region, the interannual relationship between those two variables should be consistent with the sign of that trend (e.g., if warming SSTs are responsible for decreasing precipitation, the interannual correlation should be negative). Prior to investigating that, however, we need to identify the regions in which this SST change is large relative to the magnitude of interannual SST variability (otherwise the change signal will be lost) and also to compare the model correlations with the observed correlations in order to assess the realism of the model.

Figure 11a shows the normalized SST change, or the ratio of the absolute value of the change to the interannual standard deviation, for March–May. The SST interannual variability is large compared to the long-term change in the central to eastern tropical Pacific, while the change is relatively large—and thus apt to be important in forcing a corresponding change in precipitation—in the western Pacific and Indian Oceans.

Simultaneous observed and simulated detrended 1979–2012 correlations of March–May Horn precipitation with SST and 200-mb vector winds (1 mb = 1 hPa) are shown in Fig. 12. A two-sided t test implies significance at the 95% level for a correlation above 0.35; therefore vector winds are plotted if the correlation with either wind component exceeds 0.35. For the model simulations (Fig. 12a), there are moderate (0.5–0.7) correlations of Horn rainfall with SST near the equator in the western-to-central Pacific and western Indian Oceans. Instead, the correlations between observed Horn precipitation and SST are quite weak everywhere (Fig. 12b). This may be due to sampling errors related to a small sample size: indeed, correlations in individual model runs vary substantially, with some runs exhibiting patterns quite similar to the ensemble mean (Fig. 12c) while others display patterns as weak as observed (Fig. 12d). On the other hand, March–May observed Horn precipitation–SST correlations for other comparable periods (1945–78 and 1911–44; not shown) are as low as for 1979–2012, which suggests that the model relationship is too strong. This discrepancy is consistent with the weak

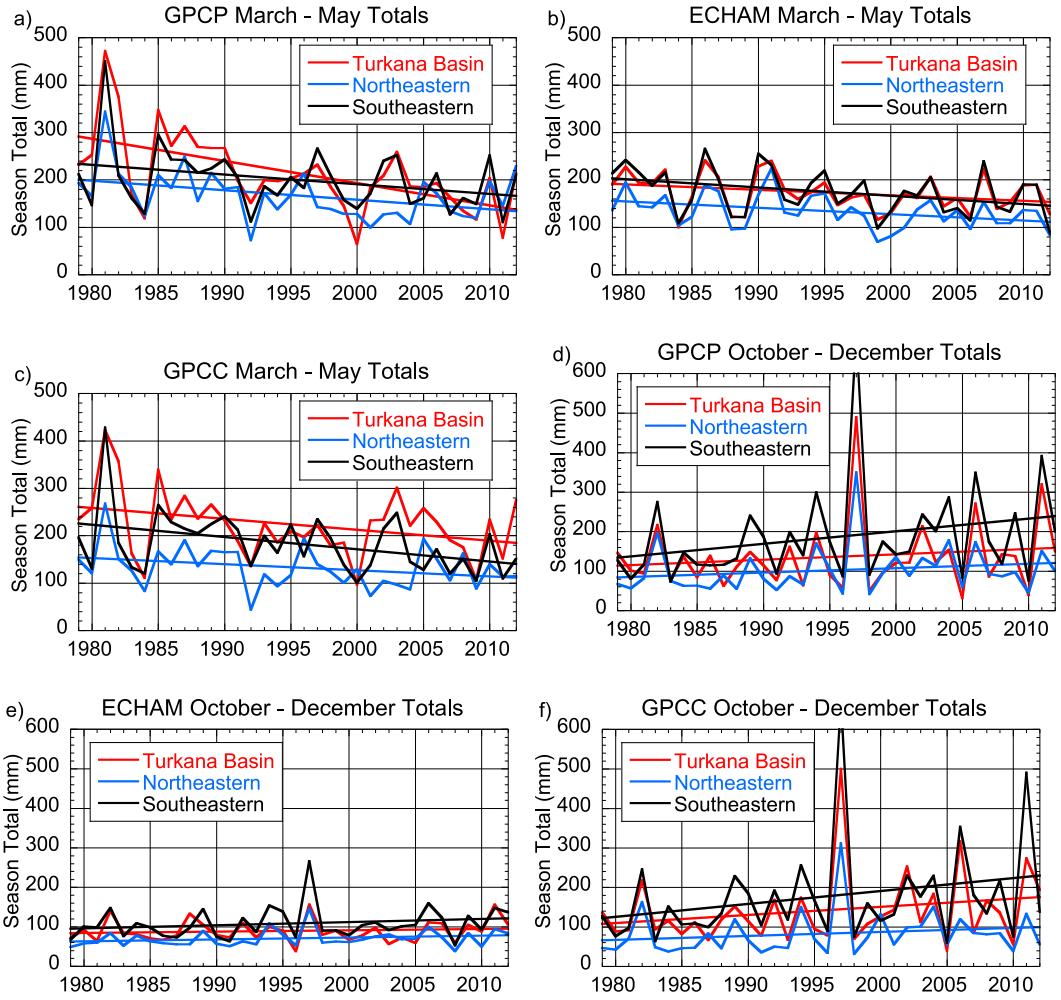

FIG. 6. Interannual seasonal rainfall averaged over grid points within regions shown in Fig. 5 (except the Ethiopian highlands) for (a) GPCP March–May, (b) ECHAM March–May, (c) GPCC March–May, (d) GPCP October–December, (e) ECHAM October–December, and (f) GPCC October–December. Lines indicate linear least squares fit.

correlation between observed and modeled Horn precipitation (Fig. 7a). A definitive answer to the question of whether the lack of correspondence between the simulated and observed correlations is due to sampling or the absence of any real covariability cannot be given but, as will be shown below, the comparison between model and observations improves when using other metrics.

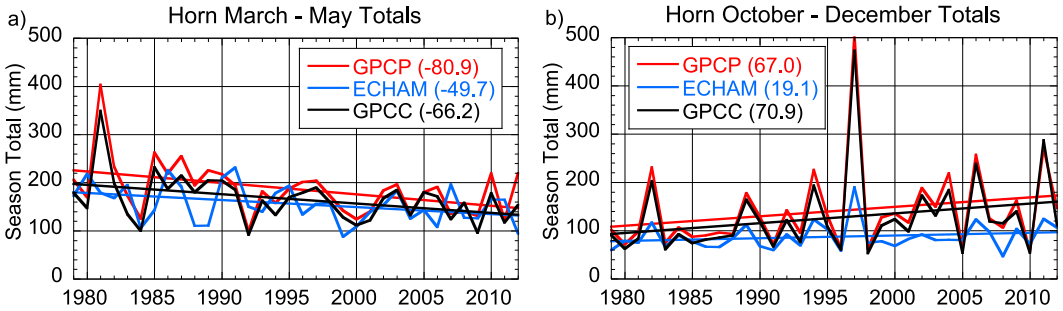

FIG. 7. Interannual rainfall averaged over the Horn region shown in Fig. 1 for (a) March–May and (b) October–December. Change for each time series (mm) is indicated in the legend. The absolute value of the change exceeds that of 1000 randomized series in March–May 99.0%, 97.2%, and 98.7%, and in October–December 80.3%, 75.6%, and 83.6% for GPCP, the ECHAM ensemble average, and GPCC, respectively.

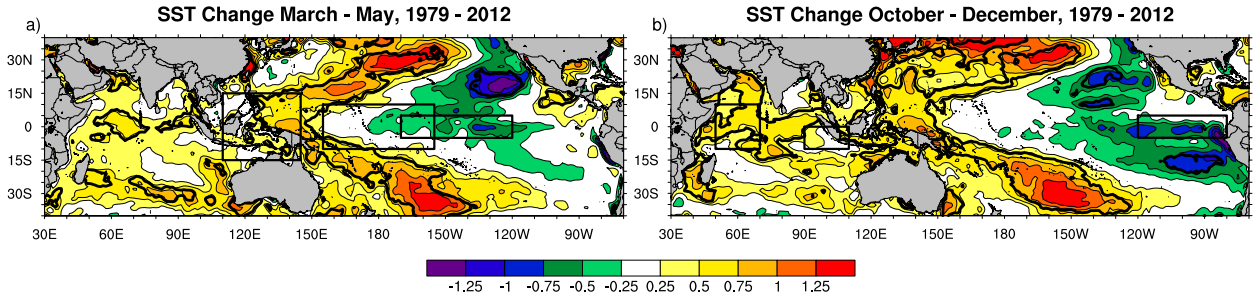

FIG. 8. SST change (defined as in Fig. 5 in degrees Celsius) from 1979 to 2012 for (a) March–May [rectangle boundaries are 5°N–5°S, 170°–120°W (Niño-3.4); 10°N–10°S, 155°E–155°W; and 15°N–15°S, 110°–145°E] and (b) October–December (rectangle boundaries are 5°N–5°S, 120°–80°W; 0°–10°S, 90°–110°E; and 10°N–10°S, 50°–70°E). Thick black curves represent the 99% statistical significance level as determined from 1000-randomization Monte Carlo test.

We now return to the issue of comparing trends and correlations by first noting that the 1979–2012 SST change has been positive (a 34-yr change of 0.42°C) in the Indo-Pacific (square centered over Indonesia in Fig. 8a) and is large compared to interannual variability (Fig. 11a), suggesting that oceanic warming there may be related to the Horn drying trend. On interannual time scales, the simulated negative correlation between March–May Horn rainfall and SSTs in this region (Fig. 12a) likewise implies that warm interannual Indo-Pacific SST anomalies are associated with drought conditions in the Horn (i.e., the sign of the trends and the interannual correlation is consistent). In the central Pacific (rectangle centered on the date line in Fig. 8a), March–May SST change has been near zero. Farther east, SSTs have cooled (e.g., the Niño-3.4 change is −0.41°C), but in this region the SST change is much smaller than interannual variability (recall Fig. 11a), so even though we might expect a related decrease in Horn precipitation on the basis of the strong positive correlations (Fig. 12a), the signal should be dwarfed compared to year-to-year variations.

Moreover, the effect that these various Pacific SST conditions have on eastern Africa March–May rainfall may represent not so much the isolated impact from any single region as the collective effect associated with changes in the zonal SST gradient between the western and central Pacific. The notion that an enhanced gradient in SST is more apt to cause increased low-level convergence than uniform warming is supported by several studies of tropical climate variability. For instance, the zonal gradient of SST in the tropical Pacific has long been recognized as critical to the ENSO phenomenon, via induced changes in the Pacific cell of the Walker circulation and in the associated regions of anomalous low-level convergence (divergence) where precipitation is enhanced (decreased) (e.g., Lindzen and Nigam 1987; Hoerling et al. 2010). Likewise, in the Indian Ocean, when the entire Walker circulation shifts westward in response to an enhanced east–west SST gradient in the western Pacific, subsidence associated with the Indian Ocean cell of the Walker circulation should increase over the eastern Horn, thereby suppressing precipitation, as hypothesized in Williams and Funk (2011) and Hoell and Funk (2013, 2014). [A caveat to this argument is that Hastenrath (2000) found no evidence of a climatological Indian Ocean Walker circulation in boreal spring during 1958–97, but note that his period of study does not include the most recent 16 yr.]

To support this line of reasoning we first point out, consistent with the idea that changes in the Indo-Pacific Walker circulation affect eastern Horn precipitation, that both the model ensemble average (Fig. 12a) and observations (Fig. 12b) indicate positive correlations with the 200-mb zonal wind over the Indian Ocean (i.e., stronger easterlies when Horn precipitation is below average). Correlations with low-level winds (not shown) reveal a weaker signal of opposite sign in the model and sparse significant correlations in the observations. In keeping with these results, in the individual run in which the SST–Horn precipitation correlation resembles the ensemble average (Fig. 12c), the anomalous (westerly) zonal flow associated with a dry Horn also resembles the ensemble average, whereas the run that has weak SST–precipitation correlations (Fig. 12d) also has weak precipitation correlations with the upper-level wind. On the other hand, one could argue that the anomalous upper-level easterlies seen to the east of the Horn during periods of reduced precipitation result from reduced horizontal outflow.

Next, we present evidence that, in the model, the SST gradient between the central and western Pacific is of more importance in producing anomalous precipitation over the Horn than the SST anomalies themselves. The Indo-Pacific and central Pacific regions discussed above are used to compute the average SST prior to calculating

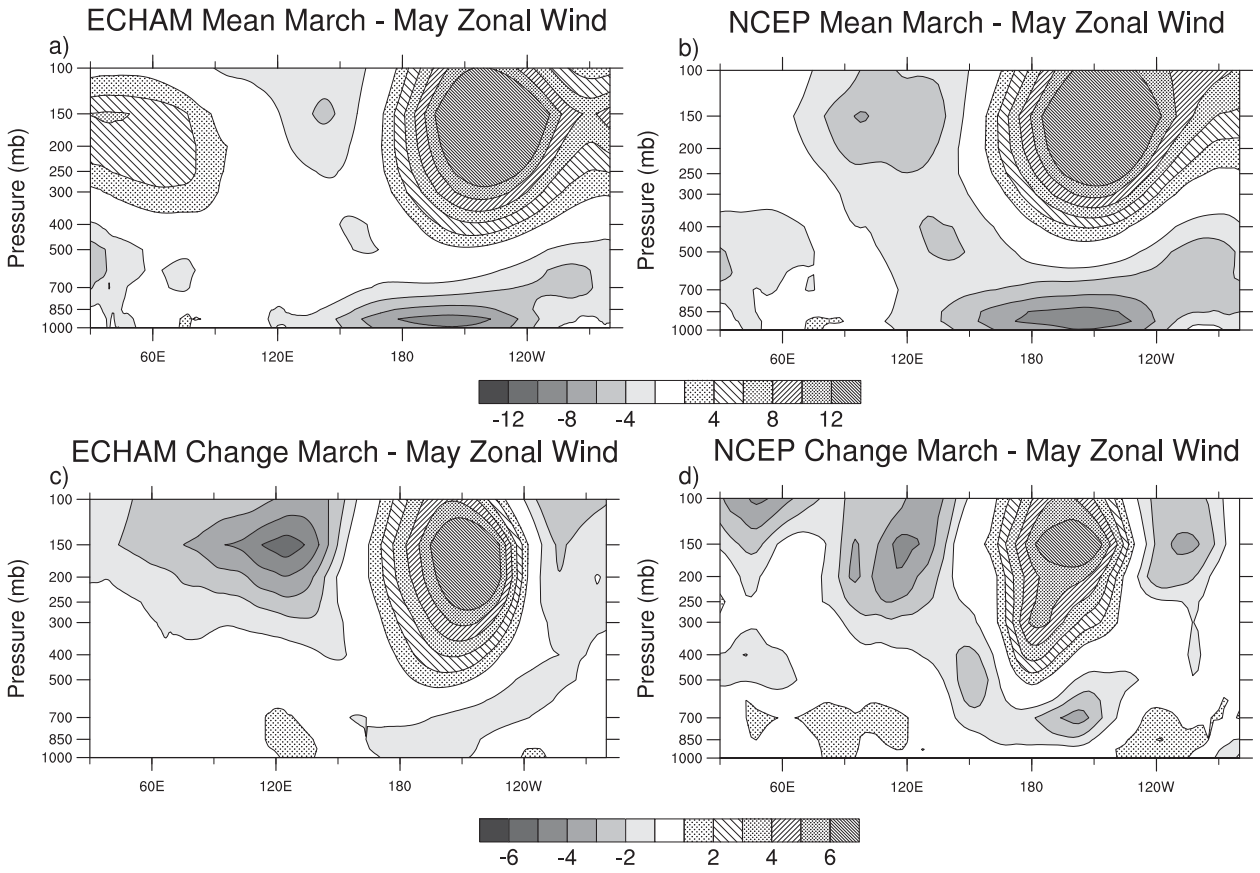

FIG. 9. Mean zonal wind (averaged from the equator to 15°N) for March–May ($m\,s^{-1}$) 1979–2012 for (a) the ECHAM ensemble average and (b) NCEP. (c) As in (a), but for change (defined as in Fig. 5). (d) As in (c), but for NCEP.

an index of the west minus east difference. The correlation between this SST gradient index and ensemble-mean Horn precipitation is a highly significant −0.74. Thus, in the ECHAM5 model, a strengthened east–west SST gradient is associated with reduced Horn rainfall. To again provide a complete comparison between the model and the observations, Fig. 13a shows the distribution of individual correlations in the model ensemble. The median is −0.42, substantially lower than the ensemble average. The spread is large with correlations ranging from −0.78, near the ensemble average, to −0.01. The observed value is −0.22, which again puts the observations within the model range but at a low probability state.

Now recall that, concurrent with the drying trend in the Horn, the March–May SST gradient has increased in the western Pacific over the 1979–2012 period: the average gradient is 0.33°C higher in the post-1995 half of the record than in the first half (see also Fig. 8a). Overall then, both the simulated and observed interannual correlations provide support for the hypothesis that the observed intensification of the March–May SST gradient in the western Pacific has contributed to the decline in Horn precipitation, via a strengthening of the convection over Indonesia and associated Indian Ocean upper-level easterlies (Fig. 9) and of the subsidence in the descending branch of the Indian Ocean Walker cell. Furthermore, the change in SST gradient seems to have occurred mostly since the mid-1990s (not shown), in line with Lyon and DeWitt (2012)'s claim that an abrupt decline in east African March–May precipitation took place at about this time [this rapid decline is not so evident in our precipitation time series, nor in Williams and Funk (2011), but Lyon and DeWitt (2012) used a wider region that extends to 10°S].

To the extent that the physics invoked involve large-scale changes in rainfall and circulation over the Indo-Pacific sector, a more adequate and direct measure of the influence of the Indonesian branch of the Walker circulation on precipitation in the Horn region is precipitation over Indonesia itself. Figure 13b is similar to Fig. 13a, except that Horn precipitation is now correlated with precipitation averaged over the Indo-Pacific square of Fig. 12. The observed, ensemble mean, and

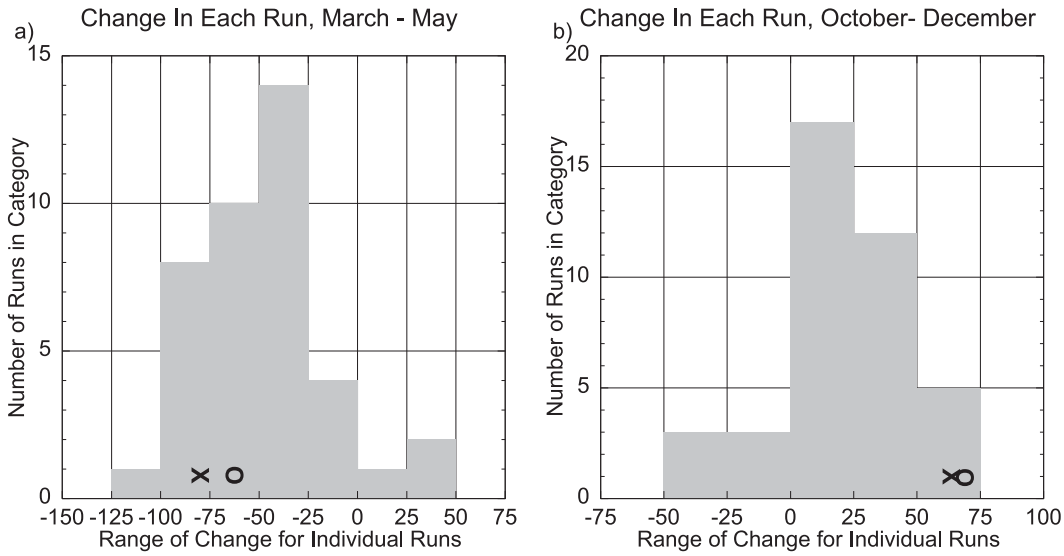

FIG. 10. Histogram of number of runs exhibiting change in the Horn region for each 25-mm category for (a) March–May and (b) October–December; The circle and cross denote GPCC and GPCP change, respectively.

median correlation improve to −0.38, −0.81, and −0.49, respectively, and the spread of the correlations is noticeably reduced compared to Fig. 13a. Thus, March–May rainfall in the Horn region tends to vary out of phase with rainfall over Indonesia in both model and observations, the linkage between them being the local Indian Ocean cell of the Walker circulation. This result lends further credence to our attribution of the Horn drying to an intensified Walker circulation in response to an increased SST gradient. The improved agreement between model and observations using this Horn–Indonesian precipitation correlation as a metric also yields a more favorable picture of the performance of the model, thus justifying its use in this study.

2) SHORT SEASON (OCTOBER–DECEMBER)

Figure 10b shows the change in Horn precipitation in each individual simulation for October–December. The modeled peak of the distribution is closer to zero than for March–May (Fig. 10a), although a majority of members (34) yield a positive trend. While the observed changes reside within the model spread, the observed precipitation increase is an extreme outcome of the model distribution. It is thus possible that the observations represent an extreme case of atmospheric noise, superimposed on a weak SST-forced signal. Of course, these inferences assume that the model response distribution is representative of nature, a premise that cannot be easily validated from the data alone.

Figure 14 shows that interannual October–December rainfall variability is related to a very different structure of SST anomalies than in March–May (Fig. 12). Moreover, the observed and simulated ensemble-mean correlation patterns are now strikingly similar. The largest positive correlations are located in the western Indian and far eastern Pacific Oceans—the latter displaying a strong ENSO signature, albeit weaker than in nature—while the largest negative correlations are found in the far eastern Indian Ocean. The rectangles in the Indian Ocean represent the poles of the IOD as defined by Saji

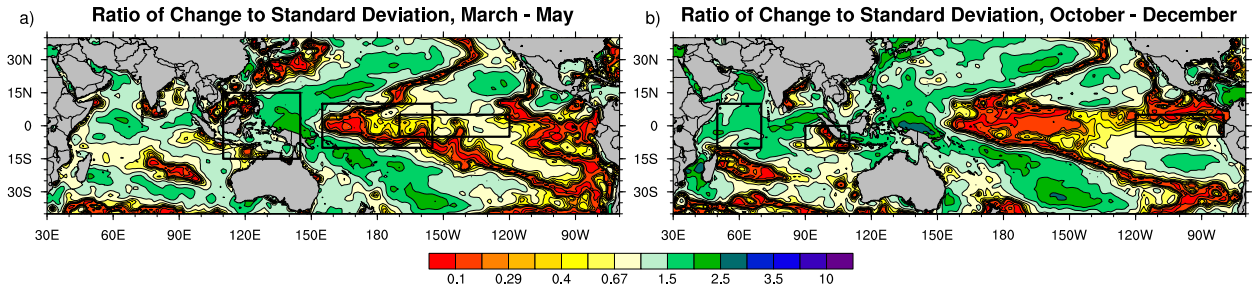

FIG. 11. Ratio of SST change (Fig. 8) to interannual standard deviation for (a) March–May and (b) October–December. Trends are included in calculations.

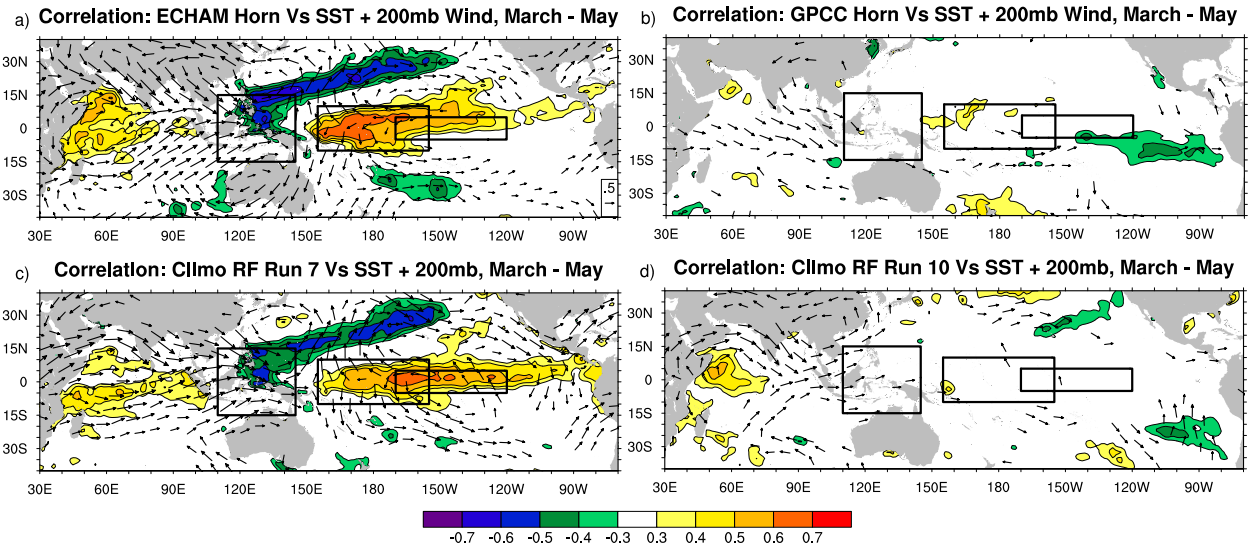

FIG. 12. Simultaneous correlation of precipitation in the Horn region with SST (shading) and 200-mb wind (vectors) for March–May: (a) ECHAM ensemble average, (b) GPCC, and (c),(d) selected runs. All data have been detrended prior to calculation. The rectangle over the Indo-Pacific region is referenced in Fig. 13. Reference vector is shown in lower right of (a).

et al. (1999) and used in subsequent studies. The correlation pattern indicates that positive precipitation anomalies in the Horn occur when the Indian Ocean west-to-east SST gradient is strong, signaling a strong IOD, consistent with many previous studies (e.g., Saji et al. 1999; Black et al. 2003; Behera et al. 2005).

The (undetrended) correlation between the IOD (average SST in the western box minus that in the eastern box) and Horn precipitation is 0.74 for the ensemble average and 0.80 in GPCC, while the correlations between SST within the eastern Pacific rectangle and Horn precipitation are 0.51 and 0.64, respectively, suggesting the dominance of the IOD. Consistent with the strong correlations between Horn rainfall and SST in both the model and observations (Fig. 14), the correlation between model and observed rainfall is 0.87 (see Fig. 7b).

The low-level wind anomalies in the Indian Ocean associated with enhanced Horn precipitation have an easterly component (Fig. 14) in both model and observations, consistent with an anomalous east-to-west SST gradient. Hastenrath et al. (2007) showed that for the short wet-season drought of 2005 the observed wind anomalies were of the opposite sign (i.e., low-level westerlies in the Indian Ocean), implying subsidence over the eastern Horn. Hastenrath et al. (1993) found a strong negative correlation ($r = -0.85$) between rainfall at the coast of East Africa and surface westerlies over the equatorial Indian Ocean during the short rainy season. Goddard and Graham (1999) who used a suite of atmospheric models forced with different configurations of SST, however, caution that these westerly winds and the Indian Ocean SSTs that appear quite important in driving Horn precipitation anomalies are themselves covariant with eastern Pacific SSTs.

The observed upward trend in October–December Horn precipitation appears to be consistent with the observed unequal warming across the Indian Ocean (Fig. 8b). Between 1979 and 2012 the western Indian Ocean SST index has increased by 0.48°C while the eastern index has increased by only 0.26°C. Given the strong positive correlation between Horn precipitation and IOD index, this change should have resulted in increased precipitation, as indeed has occurred. The observed precipitation trend, however, is inconsistent with the observed cooling in the eastern Pacific, since the positive correlations in that region (Fig. 14b) suggest that a negative SST trend should result in decreased Horn precipitation.

Note, however, that the trend in the eastern Pacific in this season is small compared to interannual fluctuations (Fig. 11b). Thus, invoking the same argument as to why SST trends in this region do not impact Horn precipitation in spring (i.e., the effect is dwarfed by that of interannual variability), we argue that the 1979–2012 changes in fall precipitation were largely controlled by the Indian Ocean SSTs, which exhibit a large normalized change and an interannual relationship with Horn precipitation of the expected sign.

4. Summary and discussion

Eastern Horn of Africa rainfall, including its seasonality, variability, and change during 1979–2012, has been

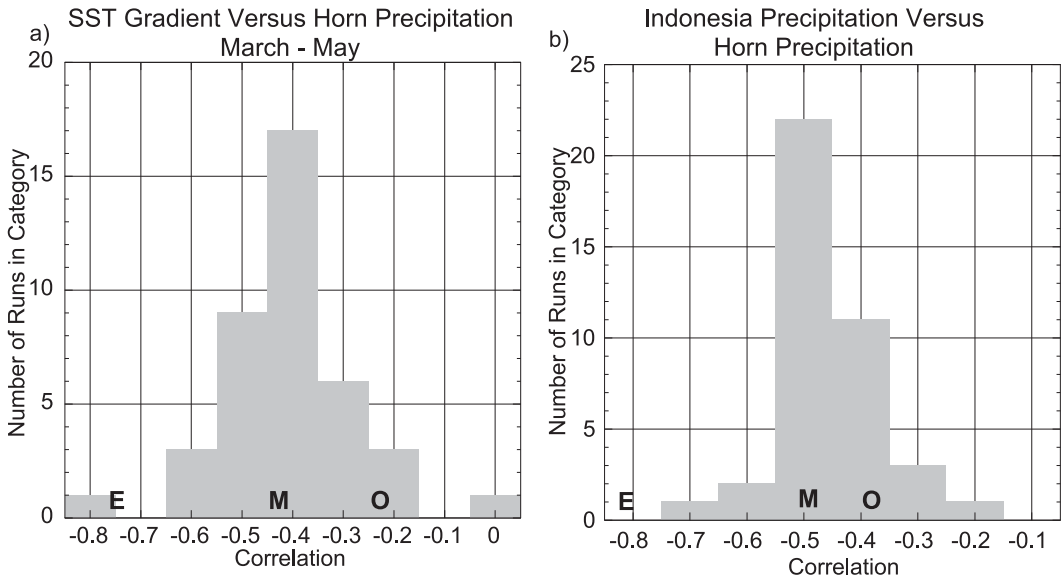

FIG. 13. Histogram showing the correlation for each of the individual ensemble members between precipitation in the Horn region and (a) the SST gradient and (b) precipitation in the rectangle representing the Indo-Pacific warm pool region shown in Fig. 12. Trends are included. In both figures the circle indicates the correlation using observations (the Indo-Pacific index in Fig. 13b is calculated from GPCP), M indicates median correlation, and E indicates ensemble average correlation.

analyzed using GPCC observations and a 40-member ensemble of ECHAM5 SST-forced atmospheric simulations. The model is deemed a particularly suitable tool for this study owing to the realism of its climatological seasonal cycle of rainfall over eastern Africa. The model is also considered an essential diagnostic tool to establish plausible causes for rainfall variations during a period in which precipitation has dramatically declined over eastern Africa.

The model's ensemble average reproduces the pronounced observed decrease in the eastern Horn of Africa's long wet season rainfall (March–May) during the recent 34-yr period, with drying in almost every individual member. The observational evidence for strong drying thus has modeling support and the model provides the additional evidence that the direction toward a decline in spring rains has been fundamentally determined by changes in SST. In contrast, the ensemble model simulates a weak, mostly statistically insignificant, increase in eastern Africa October–December short-season rains over the same 34-yr period. Observations suggest a larger absolute, as well as fractional, increase than indicated by the model.

The search for SST relationships with Horn rainfall variability and for SST attribution of observed precipitation changes was conducted via a standard analysis of the simultaneous detrended interannual correlations, combined with an assessment of the relative magnitude of SST trends and interannual variability. For the March–May model ensemble-average Horn precipitation, this analysis reveals moderate correlations, in some locations explaining up to 40% of the variance, in the central and western Pacific. Some of the largest correlations are found in a region near Indonesia that also exhibits large positive SST trends and their negative sign is consistent with the drying trend of the Horn (i.e., warm SSTs are associated with below-normal precipitation in the Horn).

The observed March–May interannual correlations between Horn precipitation and SST are small, but within the range of the individual runs, so the true SST–rainfall relationship may be stronger than suggested by the few recent decades of data. Correlations between Horn precipitation and SST for previous periods are equally weak, however, suggesting that the lack of observed correlation is not a sampling issue, but rather is indicative of the weak nature of the true relationship and implies that the model relationship is too strong. On the other hand, the detrended correlation pattern for the second half (1996–2012) of the period of interest (Fig. 15) is quite similar to the ensemble average in the Pacific (which might be the result of fortuitous sampling). Assuming 15 degrees of freedom, a correlation of 0.5 is easily significant at the 95% level using a two-sided t test. While we are fully cognizant of the dangers of using such a short period and therefore reserve judgment, it is nonetheless an intriguing correspondence.

Still, our results suggest a stronger interannual link (model ensemble-average correlation of −0.74,

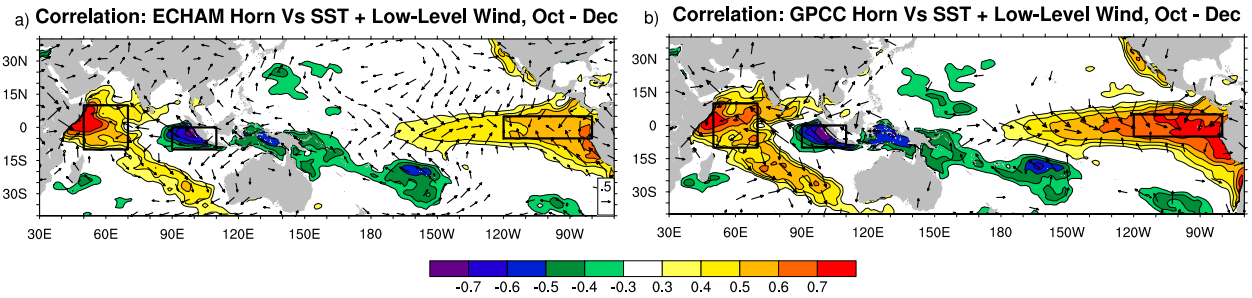

FIG. 14. As in Fig. 12, but for October–December; polygons are for the domains 10°N–10°S, 50°–70°E; 0°–10°S, 90°–110°E; and 5°N–5°S, 120°–80°W, and winds are at low level (10 m in model; 1000 mb in observations). Reference vector is shown in lower right of (a).

observed correlation of −0.22) between March–May Horn precipitation and the magnitude of the east–west SST gradient across the equatorial western Pacific than with individual centers. This finding supports the hypothesis advanced in Williams and Funk (2011) and Hoell and Funk (2013) that an enhanced zonal SST gradient induces an intensification of convection over the Indo-Pacific warm pool, which then leads to increased subsidence over eastern Africa. On the basis of these strong model correlations and the observed increase in the SST gradient, we thus view the spring Horn drying as a response to differential 1979–2012 warming in the western Pacific characterized by more pronounced warming near Indonesia. That strong observed correlations for the second half of the period (Fig. 15) coincide with the increased SST gradient is then consistent with the ''emerging'' sensitivity to the gradient as described by Hoell and Funk (2013) and Funk et al. (2013).

Considerations regarding the relative dominance of change compared to interannual variability are invoked to argue that, even though the short October–December rains are strongly positively correlated with both ENSO-related SST anomalies in the tropical eastern Pacific and with the IOD (in agreement with numerous previous studies), the 1979–2012 increase in rainfall can be mostly attributed to the warming in the western Indian Ocean. Of the three highlighted SST regions related to interannual Horn variability (Fig. 14), only in the western Indian Ocean is the SST change large compared to interannual fluctuations and the sign of the interannual correlations with Horn precipitation consistent with the observed trends. As in March–May, interannual October–December correlations between Horn precipitation and SSTs have increased for the second half of the record (not shown).

The recent increase in October–December eastern Horn rainfall also seems to be related to an enhanced SST gradient, but in this case across the Indian Ocean, as measured by the strength of the IOD. Black et al. (2003) argued that the relationship is nonlinear, because only those seasons exhibiting positive east-to-west gradients (the gradient is usually negative) have anomalous (excessive) precipitation. Nonetheless, for the recent period, the linear relationship between the dipole and Horn precipitation is strong.

A related question of great practical interest is what the model simulations suggest for the prospects of skillful seasonal forecasting of eastern Africa rainfall. Climate specialists now meet on a monthly basis to assess the East African climate outlook and generate scenarios and assumptions that food security analysts use to develop famine prevention strategies. While the necessary climate science is still being developed, the consistent ECHAM5 SST–Horn rainfall relationships explored here may eventually help to provide improved early warning.

Our interpretation of the observed post-1979 eastern Africa March–May downward rainfall trend is that the drying was a deterministic response to the SST forcing, insofar as over 90% of the 40 individual runs subjected to observed SST changes (and external radiative forcing) simulated a drying trend, although the magnitude of the drying is substantially influenced by random atmospheric variability, as implied by the fact that the observed interannual correlations are low (weaker than 0.3). The salient characteristic of the SST anomalies conducive to March – May eastern Africa drying in our model simulations is a zonal gradient in the equatorial west to central Pacific. The warming that has occurred since 1979 is also characterized by a greater warming of the western Pacific relative to the central Pacific, which should have strengthened the atmospheric Walker circulation and enhanced the drying beneath its descending East African branch. Our results thus build on the existing evidence for a mainly Pacific-basin cause for the recent decline in Horn long season rains (Lyon and DeWitt 2012; Hoell and Funk 2013, 2014). Also, contrary to recent studies proposing that the Indian Ocean exerts a primary influence on East African rainfall on multidecadal and longer time scales (Tierney et al. 2013), SST changes since 1979 in the Indian Ocean do not appear to have been the major

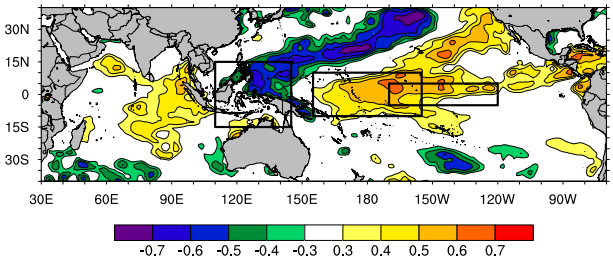

FIG. 15. As in Fig. 12b, but for 1996–2012.

driver of the recent spring drying trend over the Horn region.

A quantitative evaluation of the extent to which recent East African March–May drying originated from mostly natural decadal ocean variability or resulted from human-induced changes in ocean conditions cannot be provided by this analysis alone. The pattern of observed SST changes since 1979, with a steeper zonal gradient between the central and western Pacific Ocean (Fig. 8), to which our model simulations responded with East Africa drying, closely resembles the long-term trend pattern observed since 1901 (e.g., Compo and Sardeshmukh 2010; Solomon and Newman 2012). Evidence indicates that intrinsic natural decadal variability (e.g., Dai 2013; Lyon et al. 2013) has increased the gradient by cooling the central Pacific. A new modeling study with the Community Atmosphere Model, version 5 (CAM5; Funk and Hoell 2014, manuscript submitted to *J. Climate*), driven with SST changes associated with the first empirical orthogonal function of 1900–2012 SST after the influence of ENSO has been removed using regression (characterized by an SST gradient in the western Pacific), indicates that both components can enhance subsidence and force drying over East Africa, via the same Walker cell mechanism that appears to operate in our model.

A qualitative argument is nonetheless defensible, namely that the observed March–May Horn drying since 1979 has resulted from the region's sensitivity to a pattern of differential SST warming related to both long-term climate change and natural decadal variability. Such a view is consistent with a recent modeling study of the 2011 East African drought by Lott et al. (2013), who argue that human influences increase the odds that the long rains will be below average. The magnitude of that effect, however, was found to be sensitive to the exact pattern of SST change that was employed in their modeling experiments, again emphasizing the importance of better understanding the precise nature of the SST forcing itself.

An increased west-versus-east tropical Pacific warming is also present in the pattern of SST change observed since 1901 (not shown) and this can be contrasted with the response of coupled ocean–atmosphere models to historical forcing [i.e., simulations from phases 3 and 5 of the Coupled Model Intercomparison Project (CMIP3 and CMIP5)], which is spatially more uniform (e.g., DiNezio et al. 2009; Hoerling et al. 2010). Thus, it remains an open question to what extent the long-term observed changes in Pacific SST since 1901 reflect human-induced climate change. More research will be needed to explain the observed centennial SST trends and reconcile them with the expected effects of anthropogenic forcing. Resolving the discrepancies between centennial SST trends and CMIP5 predictions will help elucidate the relative contributions of natural variability and anthropogenic change. Recent studies with CMIP-forced regional models (e.g., Cook and Vizy 2012, 2013) report rainfall-reducing changes in Congo basin/Somali jet moisture transports and substantially shorter crop growing seasons. Future analysis could perhaps combine the types of historical AGCM analyses presented here, or AGCM trend experiments (Funk and Hoell 2014, manuscript submitted to *J. Climate*) with regional climate model simulations to better understand the plausible trajectory and long-term change of precipitation in this drought-sensitive region under global warming.

Another interesting unanswered question awaiting further research arises from the qualitative similarities in the SST change patterns for the two seasons (Fig. 8). It is not known whether the opposite sign of the Horn precipitation changes arises from differences in circulation climatologies, and therefore different sensitivities to SST changes, or from differences in the details of SST changes.

Acknowledgments. IB was funded by Grants DEVIAJE CGL2009-06944 and COMETH CGL 2012-30641 of the Spanish MICINN.

REFERENCES

Adler, R. F., and Coauthors, 2003: The version-2 Global Precipitation Climatology Project (GPCP) Monthly Precipitation Analysis (1979–present). *J. Hydrometeor.,* **4,** 1147–1167, doi:10.1175/1525-7541(2003)004<1147:TVGPCP>2.0.CO;2.

Behera, S. K., J.-J. Luo, S. Masson, P. Delecluse, S. Gualdi, A. Navarra, and T. Yamagata, 2005: Paramount impact of the Indian Ocean dipole on the East African short rains: A CGCM study. *J. Climate,* **18,** 4514–4530, doi:10.1175/JCLI3541.1.

Black, E., J. Slingo, and K. R. Sperber, 2003: An observational study of the relationship between excessively strong short rains in coastal East Africa and Indian Ocean SST. *Mon. Wea. Rev.,* **131,** 74–94, doi:10.1175/1520-0493(2003)131<0074:AOSOTR>2.0.CO;2.

Camberlin, P., and N. Philippon, 2002: The East African March–May rainy season: Associated atmospheric dynamics and predictability over the 1968–97 period. *J. Climate,* **15,** 1002–1019, doi:10.1175/1520-0442(2002)015<1002:TEAMMR>2.0.CO;2.

——, and R. E. Okoola, 2003: The onset and cessation of the ''long rains'' in eastern Africa and their interannual variability. *Theor. Appl. Climatol.,* **75,** 43–54, doi:10.1007/s00704-002-0721-5.

Compo, G. P., and P. D. Sardeshmukh, 2010: Removing ENSO-related variations from the climate record. *J. Climate,* **23,** 1957–1978, doi:10.1175/2009JCLI2735.1.

Cook, K. H., and E. K. Vizy, 2012: Impact of climate change on mid-twenty-first century growing seasons in Africa. *Climate Dyn.,* **39,** 2937–2955, doi:10.1007/s00382-012-1324-1.

——, and ——, 2013: Projected changes in East African rainy seasons. *J. Climate,* **26,** 5931–5948, doi:10.1175/JCLI-D-12-00455.1.

Dai, A., 2013: The influence of the inter-decadal Pacific oscillation on U.S. precipitation during 1923–2010. *Climate Dyn.,* **41,** 633–646, doi:10.1007/s00382-012-1446-5.

DiNezio, P. N., A. C. Clement, G. A. Vecchi, B. J. Soden, B. P. Kirtman, and S. K. Lee, 2009: Climate response of the equatorial Pacific to global warming. *J. Climate,* **22,** 4873–4892, doi:10.1175/2009JCLI2982.1.

Funk, C., and J. P. Verdin, 2010: Real-time decision support systems: The Famine Early Warning System Network. *Satellite Rainfall Applications for Surface Hydrology,* M. Gebremichael and F. Hossain, Eds., Springer, 295–320.

——, G. Senay, A. Asfaw, J. Verdin, J. Rowland, J. Michaelsen, D. Korecha, and R. Choularton, 2005: Recent drought tendencies in Ethiopia and equatorial-subtropical eastern Africa. U.S. Agency for International Development, 12 pp. [Available online at pdf.usaid.gov/pdf_docs/PNADH997.pdf.]

——, M. D. Dettinger, J. C. Michaelsen, J. P. Verdin, M. E. Brown, M. Barlow, and A. Hoell, 2008: Warming of the Indian Ocean threatens eastern and southern African food security but could be mitigated by agricultural development. *Proc. Natl. Acad. Sci. USA,* **105,** 11 081–11 086, doi:10.1073/pnas.0708196105.

——, J. Michaelsen, and M. Marshall, 2012: Mapping recent decadal climate variations in precipitation and temperature across eastern Africa and the Sahel. *Remote Sensing of Drought: Innovative Monitoring Approaches,* B. Wardlow, M. Anderson, and J. Verdin, Eds., CRC Press, 331–358.

——, and Coauthors, 2013: Attribution of 2012 and 2003–12 rainfall deficits in eastern Kenya and southern Somalia [in ''Explaining Extreme Events of 2012 from a Climate Perspective'']. *Bull. Amer. Meteor. Soc.,* **94,** S45–S48.

Goddard, L., and N. E. Graham, 1999: Importance of the Indian Ocean for simulating precipitation anomalies over eastern and southern Africa. *J. Geophys. Res.,* **104,** 19 099–19 116, doi:10.1029/1999JD900326.

Hastenrath, S., 2000: Zonal circulations over the equatorial Indian Ocean. *J. Climate,* **13,** 2746–2756, doi:10.1175/1520-0442(2000)013<2746:ZCOTEI>2.0.CO;2.

——, A. Nicklis, and L. Greischar, 1993: Atmospheric–hydrospheric mechanisms of climate anomalies in the western equatorial Indian Ocean. *J. Geophys. Res.,* **98,** 20 219–20 235, doi:10.1029/93JC02330.

——, D. Polzin, and C. Mutai, 2007: Diagnosing the 2005 drought in equatorial East Africa. *J. Climate,* **20,** 4628–4637, doi:10.1175/JCLI4238.1.

Hendon, H. H., 1986: The time-mean flow and variability in a nonlinear model of the atmosphere with tropical diabatic forcing. *J. Atmos. Sci.,* **43,** 72–88, doi:10.1175/1520-0469(1986)043<0072:TTMFAV>2.0.CO;2.

Hoell, A., and C. Funk, 2013: The ENSO-related West Pacific sea surface temperature gradient. *J. Climate,* **26,** 9545–9562, doi:10.1175/JCLI-D-12-00344.1.

——, and ——, 2014: Indo-Pacific sea surface temperature influences on failed consecutive rainy seasons over eastern Africa. *Climate Dyn.,* **43,** 1645–1660, doi:10.1007/s00382-013-1991-6.

Hoerling, M., J. Hurrell, J. Eischeid, and A. Phillips, 2006: Detection and attribution of twentieth-century northern and southern African rainfall change. *J. Climate,* **19,** 3989–4008, doi:10.1175/JCLI3842.1.

——, J. Eischeid, and J. Perlwitz, 2010: Regional precipitation trends: Distinguishing natural variability from anthropogenic forcing. *J. Climate,* **23,** 2131–2145, doi:10.1175/2009JCLI3420.1.

Huffman, G. J., and Coauthors, 1997: The Global Precipitation Climatology Project (GPCP) combined precipitation datasets. *Bull. Amer. Meteor. Soc.,* **78,** 5–20, doi:10.1175/1520-0477(1997)078<0005:TGPCPG>2.0.CO;2.

——, R. F. Adler, D. T. Bolvin, and G. Gu, 2009: Improving the global precipitation record: GPCP version 2.1. *Geophys. Res. Lett.,* **36,** L17808, doi:10.1029/2009GL040000.

Hurrell, J. W., J. J. Hack, D. Shea, J. M. Caron, and J. Rosinski, 2008: A new sea surface temperature and sea ice boundary dataset for the Community Atmosphere Model. *J. Climate,* **21,** 5145–5153, doi:10.1175/2008JCLI2292.1.

Hutchinson, P., 1992: The Southern Oscillation and prediction of ''Der'' season rainfall in Somalia. *J. Climate,* **5,** 525–531, doi:10.1175/1520-0442(1992)005<0525:TSOAPO>2.0.CO;2.

Indeje, M., F. H. M. Semazzi, and L. J. Ogallo, 2000: ENSO signals in East African rainfall seasons. *Int. J. Climatol.,* **20,** 19–46, doi:10.1002/(SICI)1097-0088(200001)20:1<19::AID-JOC449>3.0.CO;2-0.

Kanamitsu, M., W. Ebisuzaki, J. Woollen, S.-K. Yang, J. J. Hnilo, M. Fiorino, and G. L. Potter, 2002: NCEP–DOE AMIP-II Reanalysis (R-2). *Bull. Amer. Meteor. Soc.,* **83,** 1631–1643, doi:10.1175/BAMS-83-11-1631.

Kiladis, G. N., and H. F. Diaz, 1989: Global climatic anomalies associated with extremes in the Southern Oscillation. *J. Climate,* **2,** 1069–1090, doi:10.1175/1520-0442(1989)002<1069:GCAAWE>2.0.CO;2.

L'Heureux, M. L., S. Lee, and B. Lyon, 2013: Recent multidecadal strengthening of the Walker circulation across the tropical Pacific. *Nat. Climate Change,* **3,** 571–576, doi:10.1038/nclimate1840.

Liebmann, B., I. Bladé, G. N. Kiladis, L. M. V. Carvalho, G. B. Senay, D. Allured, S. Leroux, and C. Funk, 2012: Seasonality of African precipitation from 1996 to 2009. *J. Climate,* **25,** 4304–4322, doi:10.1175/JCLI-D-11-00157.1.

Lindzen, R. S., and S. Nigam, 1987: On the role of sea surface temperature gradients in forcing low-level winds and convergence in the tropics. *J. Atmos. Sci.,* **44,** 2418–2436, doi:10.1175/1520-0469(1987)044<2418:OTROSS>2.0.CO;2.

Lott, F. C., N. Christidis, and P. A. Stott, 2013: Can the 2011 East African drought be attributed to human-induced climate change? *Geophys. Res. Lett.,* **40,** 1177–1181, doi:10.1002/grl.50235.

Lyon, B., and D. G. DeWitt, 2012: A recent and abrupt decline in the East African long rains. *Geophys. Res. Lett.,* **39,** L02702, doi:10.1029/2011GL050337.

——, A. G. Barnston, and D. G. DeWitt, 2013: Tropical Pacific forcing of a 1998–1999 climate shift: Observational analysis and climate model results for the boreal spring season. *Climate Dyn.,* **43,** 893–909, doi:10.1007/s00382-013-1891-9.

Manatsa, D., and S. K. Behera, 2013: On the epochal strengthening in the relationship between rainfall of East Africa and IOD. *J. Climate,* **26,** 5655–5673, doi:10.1175/JCLI-D-12-00568.1.

Mason, S. J., and L. Goddard, 2001: Probabilistic precipitation anomalies associated with ENSO. *Bull. Amer. Meteor.*

Soc., **82,** 619–638, doi:10.1175/1520-0477(2001)082<0619:PPAAWE>2.3.CO;2.

Ogallo, L. J., J. E. Janowiak, and M. S. Halpert, 1988: Teleconnection between seasonal rainfall over East Africa and global sea surface temperature anomalies. *J. Meteor. Soc. Japan,* **66,** 807–822.

Rayner, N. A., E. B. Horton, D. E. Parker, C. K. Folland, and R. B. Hackett, 1996: Version 2.2 of the global sea ice and sea surface temperature data set, 1903–1994. Met Office Climate Research Tech. Note CRTN 74, 21 pp.

Reynolds, R. W., N. A. Rayner, T. M. Smith, D. C. Stokes, and W. Wang, 2002: An improved in situ and satellite SST analysis for climate. *J. Climate,* **15,** 1609–1625, doi:10.1175/1520-0442(2002)015<1609:AIISAS>2.0.CO;2.

Roeckner, E., and Coauthors, 2006: Sensitivity of simulated climate to horizontal and vertical resolution in the ECHAM5 atmosphere model. *J. Climate,* **19,** 3771–3791, doi:10.1175/JCLI3824.1.

Saji, N. H., B. N. Goswami, P. N. Vinayachandran, and T. Yamagata, 1999: A dipole mode in the tropical Indian Ocean. *Nature,* **401,** 360–363.

Schneider, U., A. Becker, A. Meyer-Christoffer, M. Ziese, and B. Rudolf, 2011: Global precipitation analysis products of the GPCC. Global Precipitation Climatology Centre (GPCC), DWD, 12 pp. [Available online at ftp://ftp-anon.dwd.de/pub/data/gpcc/PDF/GPCC_intro_products_2008.pdf.]

——, ——, P. Finger, A. Meyer-Christoffer, M. Ziese, and B. Rudolf, 2014: GPCC's new land surface precipitation climatology based on quality-controlled in situ data and its role in quantifying the global water cycle. *Theor. Appl. Climatol.,* **115,** 15–40, doi:10.1007/s00704-013-0860-x.

Shepard, D., 1968: A two-dimensional interpolation function for irregularly spaced data. *Proc. 23rd ACM National Conf.,* Las Vegas, NV, Association for Computing Machinery, 517–524.

Shinoda, T., M. A. Alexander, and H. H. Hendon, 2004: Remote response of the Indian Ocean to interannual SST variations in the tropical Pacific. *J. Climate,* **17,** 362–372, doi:10.1175/1520-0442(2004)017<0362:RROTIO>2.0.CO;2.

Solomon, A., and M. Newman, 2012: Reconciling disparate twentieth-century Indo-Pacific ocean temperature trends in the instrumental record. *Nat. Climate Change,* **2,** 691–699, doi:10.1038/nclimate1591.

Tierney, J. E., J. E. Smerdon, K. J. Anchukaitis, and R. Seager, 2013: Multidecadal variability in East African hydroclimate controlled by the Indian Ocean. *Nature,* **493,** 389–392, doi:10.1038/nature11785.

Ummenhofer, C. C., A. Sen Gupta, M. H. England, and C. J. C. Reason, 2009: Contributions of Indian Ocean sea surface temperatures to enhanced East African rainfall. *J. Climate,* **22,** 993–1013, doi:10.1175/2008JCLI2493.1.

Viste, E., D. Korecha, and A. Sorteberg, 2013: Recent drought and precipitation tendencies in Ethiopia. *Theor. Appl. Climatol.,* **112,** 535–551, doi:10.1007/s00704-012-0746-3.

Wang, B., Q. Ding, X. Fu, I.-S. Kang, K. Jin, J. Shukla, and F. Doblas-Reyes, 2005: Fundamental challenge in simulation and prediction of summer monsoon rainfall. *Geophys. Res. Lett.,* **32,** L15711, doi:10.1029/2005GL022734.

Webster, P. J., A. M. Moore, J. P. Loschnigg, and R. R. Leben, 1999: Coupled ocean–atmosphere dynamics in the Indian Ocean during 1997–98. *Nature,* **401,** 356–360, doi:10.1038/43848.

Williams, A. P., and C. Funk, 2011: A westward extension of the warm pool leads to a westward extension of the Walker circulation, drying eastern Africa. *Climate Dyn.,* **37,** 2417–2435, doi:10.1007/s00382-010-0984-y.

Willmott, C. J., C. M. Rowe, and W. D. Philpot, 1985: Small-scale climate maps: A sensitivity analysis of some common assumptions associated with grid-point interpolation and contouring. *Amer. Cartogr.,* **12,** 5–16, doi:10.1559/152304085783914686.